Studies on the Growth and Characterization of Rare-Earth Gd-Doped InGaN/GaN Magnetic Semiconductor Heterostructures

（希土類 Gd 添加 InGaN/GaN 磁性半導体ヘテロ構造の成長と評価に関する研究）

Mohd Tawil Siti Nooraya

Osaka University

January 2011

Abstract

Spintronics is an emerging field in which the spin of carriers in addition to the charge of carriers can be used to achieve new functionalities in electronic devices. The availability of materials exhibiting ferromagnetism above room temperature is prerequisite for realizing such devices. Materials suitable for spintronic applications are desired to be compatible with conventional growth and fabrication techniques in addition to exhibiting above room temperature ferromagnetic properties.

In this research, the growth of InGaGdN epilayers have been achieved on (0001) sapphire substrates or metalorganic vapor phase epitaxy (MOVPE)-grown GaN/sapphire templates by plasma-assisted molecular beam epitaxy (MBE) using elemental Ga, In, Gd and Si (co-doping) and gaseous N_2 as sources. Magnetic characterization of the grown epilayers was performed by a superconducting quantum interference device (SQUID) magnetometer. Ferromagnetic properties were observed at room temperature for this new type of quaternary alloy material. Co-doping of InGaGdN with Si was performed and increase in shallow donor density as well as enhancement in ferromagnetic properties were achieved. Luminescence properties of InGaGdN were also observed at room temperature with the emission peak energy red-shifts corresponding to the InN molar fraction. Gd incorporation into InGaN epilayers were confirmed by X-ray absorption fine structure (XAFS) analysis revealing that Gd^{3+} ions substitutionally occupy the cation sites of Ga of host material.

MBE growth of multi-layer structures i.e. InGaGdN/GaN multiple-quantum well (MQW) was also carried out and its characteristic were investigated. The InGaGdN/GaN MQW samples showed clear hysteresis and clear saturation in the magnetization versus magnetic field curve with larger magnetization per unit volume than the InGaN/GaGdN MQW samples implying that carrier (electron) induced ferromagnetism occurs in such heterostructures. Better structural qualities have been achieved for the Si-doped barrier layers of InGaGdN/GaN samples in which more pronounced satellite peaks can be observed from the X-ray diffraction curves compared to the undoped barrier sample.

Adding Si in the barrier layers has further enhanced the ferromagnetic properties as well as electrical properties of the MQW structure samples.

This work has provided useful experimentally based insights into GaN-based diluted magnetic semiconductors (DMSs), resulting in the development of semiconducting materials that show room temperature ferromagnetism. These materials could pave the way for development of multifunctional microelectronic devices that integrate electrical, optical, and magnetic properties particularly for the development of spin-based-electronic devices.

Contents

Chapter 1

Introduction

The evolution of magnetic materials has primarily focused on metallic 3*d* transition elements such as: Fe, Ni, Co, etc. These elements have been alloyed to create ferromagnetic compounds having a diversity of magnetic properties and applications. The most essential magnetic properties for the purpose of device applications are the Curie temperature (T_C), saturation magnetization (M_S) and coercivity (H_C). Concerning these issues, several ferromagnetic devices have been developed exploiting the spin of electrons to manipulate data storage. These devices operate on the concept of giant magnetoresistance (GMR) and generally making use of the spin valve configurations with applications such as read heads, magnetoresistive random access memory, and hard drives. Other applications include solenoid switches, sensors and so on. These applications rely only on the spin of electrons toward facilitating data storage, which restrict the types of devices that can be created from these materials.

Semiconductor materials such as Si, GaAs, and GaN have been used for a wide range of applications. Si and other indirect bandgap materials have been used for applications such as metal oxide semiconductor field effect transistors, diodes, bipolar junction transistors, and solar cell applications [1]. Si is the principal material used in computer applications today; thus it is often a goal to create new materials that are compatible with existing semiconductor processing techniques and technology. Direct

bandgap materials such as GaAs and GaN have been developed over the years where major applications are such as light emitting diodes (LEDs) and laser diodes (LDs) [1, 2]. Current semiconductor technology takes advantage of the charge of carriers, (i.e. via doping to get n- or p-type for electrons or holes, respectively) which makes these materials undesirable for data storage.

Mass, charge, and spin of electrons in solid state materials are the foundation for the information technology utilized today. However, most applications are separated into two groups; i.e. semiconducting and magnetic. In this regard, two different devices for data processing and storage are necessary in which they require additional processing steps for integration and will undoubtedly multiply the expenses. Besides, device efficiency can be affected by electrical loss at interfaces and connections as well as problems that might occur from stray electromagnetic radiation or heat dissipation. Obviously, those effects reduce the speed of the devices. For that reason, it is possible to produce new devices capable of data processing and storage by combining the use of both the charge and spin of electrons.

In the beginning, efforts to realize spin dependent transport were accomplished by using ferromagnetic metals as contacts in traditional semiconductor devices to facilitate spin polarized injection [3, 4]. However, these devices suffered from scattering at the metal/semiconductor interface, hence considerably reducing the spin injection to less than a few percent [5, 6]. This was attributed to the differences in the resistivity between the two different materials. This ultimately led to the research and development of a new type of material called dilute magnetic semiconductors (DMS), which was created by means of doping or alloying conventional semiconductors with a magnetic transition element. Due to this discovery, semiconductors have been categorized into three categories as shown in Fig. 1.1.

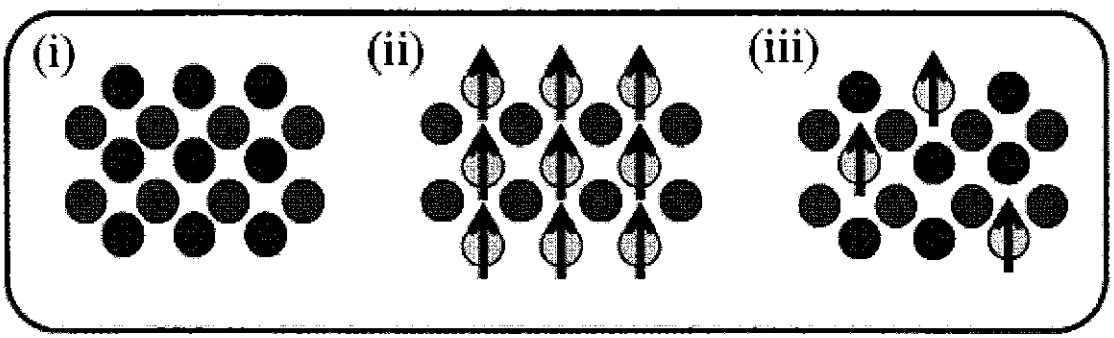

Fig. 1.1 Three types of semiconductors: (i) conventional semiconductor; (ii) magnetic semiconductors; and (iii) dilute magnetic semiconductors. (Arrows indicate magnetic atoms).

(i) Conventional semiconductor materials. These are used in most of current technological applications and are not magnetic since no magnetic ions are present. Dopants are used to change the electrical characteristics of the device. For example: Si, GaAs, GaN, Ge.

(ii) Magnetic semiconductors. These materials have both ferromagnetic and semiconducting properties, with a periodic array of magnetic elements. Materials such as semiconducting spinels and europium chalcogenides possess these properties [7].

(iii) Dilute magnetic semiconductor (DMS). These materials are created by introducing/alloying a magnetic element (impurity) into a nonmagnetic semiconductor, similar to doping. For example: (In,Mn)As, (Ga,Mn)As.

The realization of DMS materials should allow the injection of spin-polarized current into semiconductors in order to control the spin state of carriers that will contribute toward new optical and electrical devices. The capability of controlling the spin and charge in electronic devices should lead to improved efficiency, data storage, and possibility of quantum computing. The expected benefits for optical devices are the development of magnetically tunable waveguides and the ability of tuning the

wavelength through an applied magnetic field as opposed to the conventional band gap engineering. Alloying compound semiconductors such as the III-nitrides and III-arsenides with the transition element such as Mn has provided promising results for creating DMS materials. Mn has been an ideal candidate as a magnetic dopant in these materials since it can produce a moment up to 4 Bohr magneton (μ_B). In compound semiconductors such as GaAs or GaN, the Mn^{2+} ion substituting on the Ga^{3+} lattice site not only acts as a magnetic ion but also serves as p-type dopant in these materials [8-12]. Magnetic doping or alloying of III-V semiconductors to the necessary concentrations (up to 5%) presents a variety of potential obstacles for growth, such as: segregation of the magnetic impurities; difficulty exceeding the thermodynamic solubility limit; and evading the formation of secondary magnetic phases.

In 2000, theoretical studies by Dietl predicted the T_C for various p-type semiconductors doped with 5 % Mn and a hole concentration of 3.5×10^{20} cm^{-3} (Fig. 1.2) [7]. It was shown that wide bandgap semiconductors such as GaN and ZnO should have T_C greater than room temperature (RT) due to their smaller lattice constants that allow for greater p-d hybridization and reduced spin-orbit coupling. Although ZnO is a promising candidate for spintronic devices, it is still difficult to obtain good quality ZnO material and p-doping of ZnO is challenging [8]. On the other hand, the GaN-based materials already have a well established technology base for optoelectronic devices (mainly UV/blue LEDs and lasers) and electronic devices (high power FETs) into which the GaN-based DMS can be incorporated.

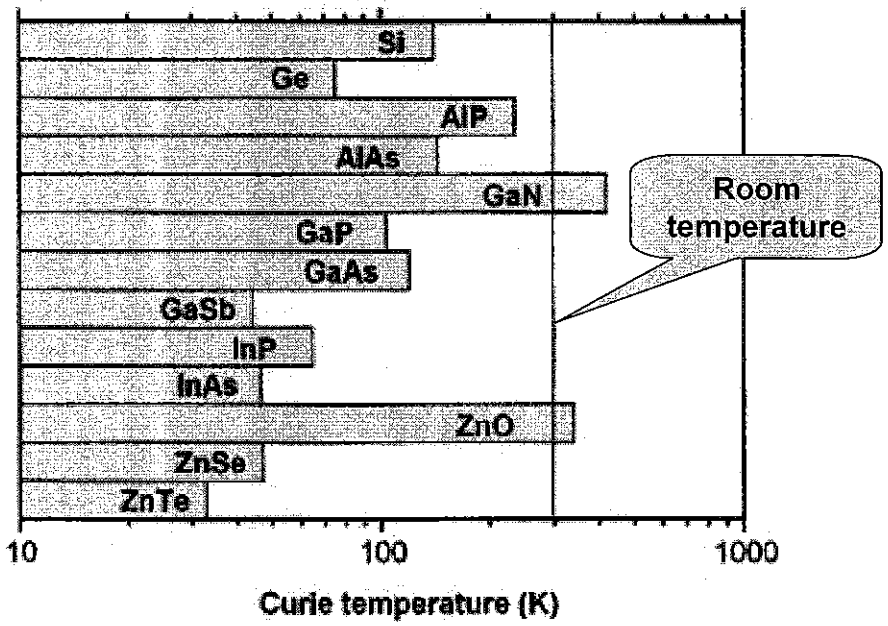

Fig. 1.2 Schematic of calculated Curie temperature (T_C) for various p-type semiconductors doped with 5 % Mn and 3.5 × 10^{20} cm^{-3} holes [7].

Since then, there has been a lot of attention in creating new nitride-based DMS materials with higher Curie temperatures by various techniques. Such DMS includes the rare-earth Gd-doping into GaN in which Teraguchi *et al.* has first reported the room temperature ferromagnetism of GaGdN that exhibits a T_C of > 400 K. Detailed account regarding the earlier prominent works on GaGdN is further described in section 1.2. In addition to GaN-based DMS, Gd-doped InGaN can also be a potential host for diluted magnetic semiconductors as it has been a notable key material for optoelectronic devices operating over a wavelength range from near-infrared to ultraviolet [9]. This research will focus on rare-earth (RE) doping of ternary alloy of InGaN in which application for spin-controlled optoelectronic devices over a longer wavelength is feasible by principally varying the In composition. This was accomplished by the molecular beam epitaxy (MBE) growth and characterization of Gd-doped InGaN epilayer, Gd-doped InGaN/GaN multiple-quantum well structures as well as investigation on the effect of Si co-doping on those semiconductor structures.

This study hopes to build the foundation of DMS material that will enable the fabrication of longer wavelength spin-based electronic (spintronic) devices such as spin-LED and circularly-polarized laser diodes. The remaining pages of this chapter will specifically describe the background study on semiconductor spintronics as well as the RE-doped III-nitride semiconductors.

1.1 Semiconductor spintronics

Spintronics is a relatively new area of research where applications are designed to manipulate the electron spin degree of freedom. Industrial devices exploiting this property are read heads and memory-storage cells, both of which use the spin valve structure [10]. These devices are typically comprised of ferromagnetic TM or RE elements and their alloys. Recently, most of the effort in spintronics was focused on improving materials for these applications. However, the discovery of DMS [11] has potential for a new class of spintronic devices; where the effort focuses on seeking ways to utilize both information processing and data storage within one material system. In these materials, a sizable number of nonmagnetic cations are replaced by magnetic ions to facilitate ferromagnetic behavior.

The first discovery of DMS material was in 1989 by Munekata *et al.* by doping InAs with Mn [11]. The material was ferromagnetic with a T_C of ~ 50 K. This material was grown by low temperature MBE growth in a temperature range of 200-300°C to prevent the formation of ferromagnetic secondary phases such as MnAs. It was found that Mn acted as an n- or p-type dopant in InAs by optimizing the growth conditions. The n-type films were found to be paramagnetic, while ferromagnetic behavior was observed in p-type samples below the Curie temperature and within the optimized Mn concentration range [12]. The existence of the ferromagnetic behavior for p-type (In,Mn)As was elucidated in terms of the formation of bound magnetic polarons. Even though it was suggested that the ferromagnetic response could be due to the magnetic

coupling between the Mn spins S caused by a local exchange J of the form $J\,S{\cdot}s$, where s is the spin of the localized holes [13]. This infers that Mn spins are coupled antiferromagnetically with the spin of the holes, thus allowing for long range ferromagnetic coupling between the Mn atoms within the lattice. The ferromagnetic origin was also explained in terms of the Ruderman-Kittel-Kasuya-Yosida (RKKY) interaction via the exchange interaction, J_{pd} [14]. However, Akai [15] proposed that the ferromagnetic properties result from competing effects of the superexchange and double exchange mechanisms acting within the material.

In 1996, Ohno and coworkers [16] discovered that Mn-doped GaAs was also ferromagnetic with a T_C of 110 K. The material was grown using low temperature MBE [11] at 250°C to avoid the formation of secondary phases, where Mn concentrations are from 1.5 to 7.1 %. The presence of Mn in GaAs produced ferromagnetic behavior as well as holes due to its acceptor nature. Later it was demonstrated that these materials must have p-type conductivity to possess ferromagnetic behavior [16-19], where the material exhibited antiferromagnetic behavior when fully compensated [21]. This led several authors to conclude that the ferromagnetic interaction within these materials was hole (or carrier) induced [20-23], and that the origin of ferromagnetic behavior could be explained by the RKKY interaction via the J_{pd}. Electron paramagnetic resonance (EPR) measurements performed on (Ga,Mn)As demonstrated the $Mn^{2+}(d^5)$ state [24].

In 1997, Koshihara [25, 26] and Munekata [27] observed ferromagnetic order by photogenerated carriers in (In,Mn)As/GaSb heterostructures. These materials were under tensile strain and demonstrated a strong perpendicular magnetic anisotropy. They verified that the strength of ferromagnetic spin exchange could be controlled by altering the hole concentration via photo-generated carriers. EPR measurements performed by Szczytko *et al.* [28] indicated that the Mn impurity in $In_{1-x}Mn_xAs$ is $Mn^{2+}(d^5)$ described as an ionized acceptor A^-. Blattner *et al.* [29] has demonstrated a Curie temperature of 333 K for (In,Mn)As grown by metal-organic chemical vapour deposition (MOCVD), for which they attributed that ferromagnetic behavior to the formation of small clusters

of a few magnetic atoms as proposed by Schilfegaarde [30]. However, no structural characterization was provided to confirm these findings reported by Blattner [29].

Earlier development of these materials has focused on doping II-VI [31-36] and III-V [10, 35-40] compound semiconductors with the TM and RE ions. Devices utilizing these types of semiconductors are expected to have many benefits over the mature technology to include signal amplification [43], multi-functional devices to include data processing and storage [44], and compatibility with today's semiconductor technology making integration more plausible [12]. In this point of view, DMS materials in which a fraction of the host cations can be substitutionally replaced by magnetic ions are of particular interest. The elements commonly used as magnetic dopants for the synthesis of DMS belong to the family of transition metals (Sc, Ti, V, Cr, Mn, Fe, Co, Ni and Cu) and rare earths (Sm, Eu, Gd, Tb, Dy and Er).

The magnetic dopants of TM or RE elements provide spin magnetic moments associated with their electron spins. A number of novel device structures have been proposed that utilize the advantage of magnetic properties of these materials. Some of these devices include the spin-LED [45, 46], spin transistor [47], magnetic sensors [48], biodetectors [49] and optical isolators [50]. Let's take a look at particular application of spin-based electronic devices such as LED. In conventional LED devices, unpolarized electrons recombine with unpolarized holes resulting in the emission of unpolarized light. In spin-LEDs, the emitted light would be polarized. This is achieved when a polarized carrier is injected from a ferromagnetic layer into a semiconductor and preferentially recombines with a carrier of opposite type and same spin orientation. Spin-up electrons would recombine with spin-up holes etc. and emit circularly polarized light (right or left).

Ohno *et al.* demonstrated the first successful spin injection in materials using a ferromagnetic semiconductor as a spin injector (Fig. 1.3) [45]. Spin-polarized holes were injected from the 300 nm thick $Ga_{0.95}Mn_{0.045}As$ (Mn in GaAs introduces holes and thus makes it p-type) under forward-bias into the $In_{0.13}Ga_{0.87}As$ QW and recombined with unpolarized electrons from the 500 nm thick n-GaAs ($N_D = 2.3 \times 10^{18}\ cm^{-3}$) substrate.

Ferromagnetic hysteresis curves were observed for temperatures up to 52 K but above this temperature GaMnAs became paramagnetic.

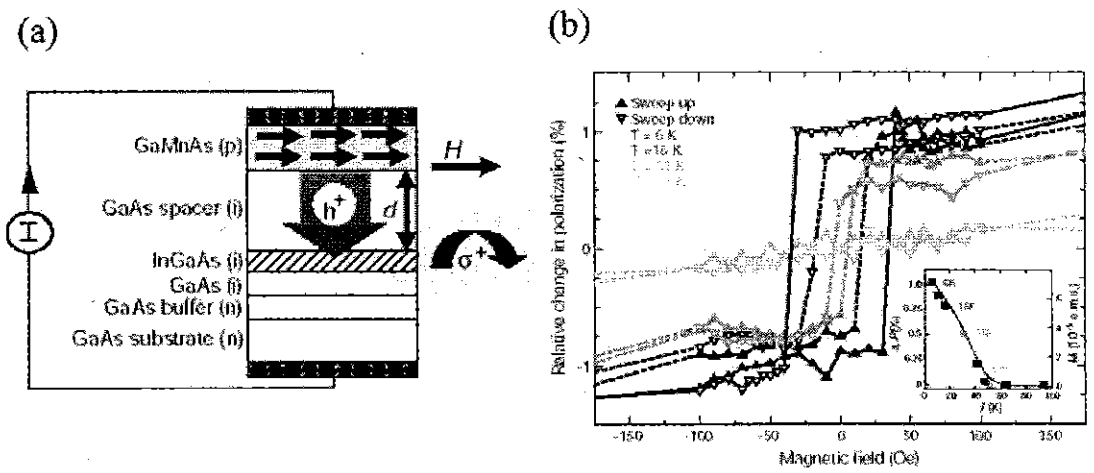

Fig. 1.3 (a) Schematic of spin-LED based on GaMnAs spin injector, (b) spin polarization efficiency as a function of applied magnetic field; inset shows the temperature dependence of the remanent polarization as a function of temperature for no applied field [45].

Recently, Ham *et al.* reported on fabrication of the nitride-based spin-LED with the ferromagnetic (Ga,Mn)N layer as a spin injection source, from which electroluminescence (EL) measurements reveal that spin-polarized electrons from the (Ga, Mn)N layer into (In,Ga)N QWs were injected even at room temperature [46]. In the heterostructure of Fig. 1.4, the (Ga,Mn)N layer is the spin injection layer and sandwiched between two n-type GaN layers because the Mn concentration in the layer is not high enough to compensate the native defects, and electrons rather than holes have long spin lifetimes and high mobilities, which are favored in high-frequency and low-power device operation. As the magnetic field is applied along the surface normal, electrons in the (Ga,Mn)N layer become spin-polarized and are injected into the (In,Ga)N quantum wells (QWs). The radiative recombination of spin-polarized carriers, which obeys well-known quantum mechanical selection rules, produces the emission of right- or left- circularly-polarized light [46].

Circular polarization of electromagnetic radiation is a polarization such that the tip of the electric field vector, at a fixed point in space, describes a circle as time progresses. The electric vector, at one point in time, describes a helix along the direction of wave propagation. The magnitude of the electric field vector is constant as it rotates. Circular polarization is feasible because the propagating electric and magnetic fields can have two orthogonal components with independent amplitudes and phases and the same frequency. A circularly polarized wave could be resolved into two linearly polarized waves, of equal amplitude, in phase quadrature (90° apart) and with their planes of polarization at right angles to each other. The circularly polarized light emission from the LED would be practical for digital optical signaling and encryption [51].

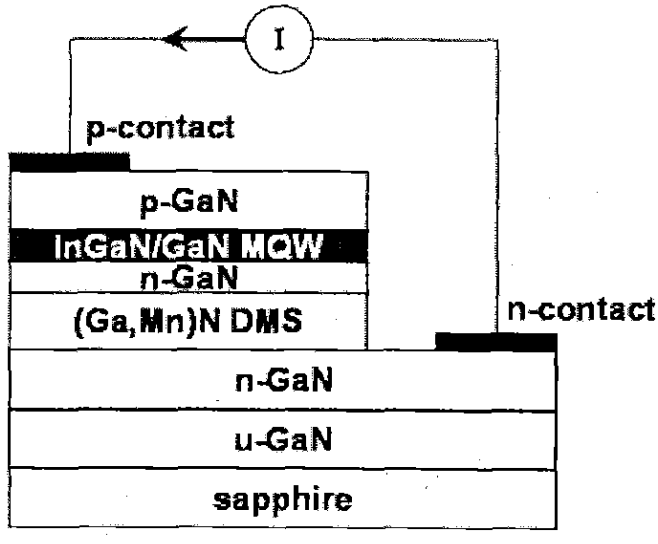

Fig. 1.4 Schematic cross section of spin-LED heterostructure with the (Ga, Mn)N layer as a spin injection source [46].

1.2 Overview on rare-earths doped III-nitride semiconductors

Rare earth (RE) elements are promising alternatives to transition metals for use in developing a DMS for potential spintronic applications. RE elements have unpaired electrons in the 4f orbitals and thus have a higher net magnetic moment as compared to TM ions. The 4f orbitals are localized and the direct coupling between the 4f ions is weak [52]. There have been several attempts of using RE elements for optoelectronic applications, as their various internal f-shell electronic transitions vary in energy from infrared to visible [53, 54]. In crystalline materials the rare earths usually exist in a 3+ charge state though occasionally as 2+ [53]. RE ions generally substitute the Ga lattice site in GaN (Fig. 1.5) [53]. Wurtzite GaN has a strong ionic bonding character and the lack of inversion symmetry results in the production of strong ligand fields that increase the probability of 4f-4f transitions that are forbidden by Laporte selections rules in the isolated ion [54]. When the RE ions are introduced into a semiconductor, the RE radiative transitions display intense intra 4f luminescence and the electron-phonon coupling is weak due to the shielding provided by the $5s^2$ and $5p^6$ electrons. It is due to this shielding that the RE 4f electronic levels are more influenced by spin-orbit coupling than by the crystal field [55].

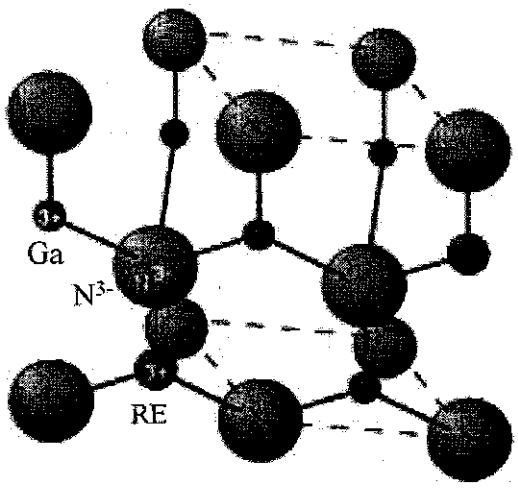

Fig. 1.5 Illustration depicting the rare-earth (RE) element incorporation in GaN [53].

The solubility of RE in GaN is much higher as compared to the Si and other narrow bandgap semiconductors. As for example, the optically active erbium concentrations ranging from 3 to 5 % have been reported in GaN [56]. Over the past few years significant effort has been made in doping GaN with RE dopants such as Eu and Er as well as Tm to develop red, green and blue electroluminescent devices [53]. GaN doped with another RE ion, i.e. Dy, has also been reported to show room temperature ferromagnetism with interesting hysteretic behavior [58].

With regards to utilizing RE ions to create a DMS, gadolinium (Gd: $4f^7\ 5d^1\ 6s^2$) is most attractive as it is the only RE ion that has both unfilled d and f orbitals. This will allow magnetic coupling through intra-ion 4f-5d exchange interaction followed by charge carrier mediated inter-ion 5d-5d coupling. Because of this, several studies have been conducted with the aim of developing ferromagnetic $Ga_{1-x}Gd_xN$ using ion implantation and molecular beam epitaxy [59-66, 71].

1.2.1 Gd-doped GaN

The first report on epitaxial $Ga_{1-x}Gd_xN$ layers was made by Teraguchi *et al.* who used RF-plasma-assisted MBE to grow the epitaxial layers on the SiC substrate [59]. They grew 250 nm of $Ga_{0.94}Gd_{0.06}N$ that displayed ferromagnetic behavior with T_C higher than 400 K, which is greater than the T_C of Gd metal (T_C = 292.5 K) and the T_C of rock salt structure GdN (T_C = 58 K) [59-62]. Their optical characterization at RT yielded an emission peak at 370 nm, which is slightly red-shifted than the bandgap luminescence of GaN (363 nm) indicating that the bandgap of GaN shrinks when Gd atoms are incorporated. A separate study on GaN bulk crystals doped with Gd by Lipinska *et al.* shows that Gd doping introduces some new features in optical characterization results [63]. Low temperature photoluminescence (PL) measurements performed at 4.2 K revealed luminescent peaks at 3.3 eV (= 370 nm) in addition to the GaN band gap. Contrary to the assignment by Teraguchi *et al.*, Lipinska *et al.* attribute these additional

peaks to a transition from the Gd^{3+} ($4f^7$) excited level, $^6P_{7/2}$, to its ground state, $^8S_{7/2}$. Additional peaks are also seen at 1.6-1.8 eV and have been attributed to Gd^{3+} transitions. These are believed to be due to transitions between $^6G_{7/2}$ to ^6P_J (J = 7/2, 5/2, 3/2) states [63].

In a study by Dhar *et al.* lightly doped (< 10^{16} cm^{-3}) $Ga_{1-x}Gd_xN$ were grown by MBE on SiC substrates. This epitaxial film appeared to be a single phase material and exhibited a very large ferromagnetic moment ~4000 μ_B/Gd atom as opposed to its atomic moment of 8 μ_B/Gd atom [64]. It also showed that based on the convergence of the field cooled (FC) and zero field cooled (ZFC) curves, the T_C was found to be 360 K. The $Ga_{1-x}Gd_xN$ films obtained were found to be highly resistive with a resistivity of 1 MΩ-cm. There is no robust theory to explain the giant magnetic moment observed in these materials, but a phenomenological model has been proposed which suggests that the long range spin polarization of the GaN matrix is caused by the strain field induced by the introduction of the Gd atom [64]. This is based on the reasoning that because Gd has a larger atomic size than Ga, it is possible that Gd substitution of Ga in GaN produces a large strain field around it. Dhar *et al.* suggest that due to the large piezoelectric coefficient of GaN along the c axis, a strain field generates a potential dip around each Gd atom. These potential minima trap the carriers locally, and if there is a spin-splitting in the band structure, the localized carriers become spin polarized [64]. It is the observation of the high magnetic moment by Dhar *et al.* that has provided force to the study of Gd-doped GaN.

MBE reports have been made by Hite *et al.* for $Ga_{1-x}Gd_xN$ grown at 700°C on sapphire substrates [65]. Their results show that doping of GaN with 10^{17} Gd atoms /cm^3 makes the host semiconductor ferromagnetic at RT and also highly resistive. This report showed that doping with Si can improve the conductivity, but the magnetization measurements did not show any significant impact of Si on saturation magnetization.

Recently, Zhou *et al.* reported that $Ga_{1-x}Gd_xN$ thin films with x = 12.5 % were obtained by MBE (growth temperature < 300°C) on sapphire substrates by [66]. X-ray

diffraction (XRD) results showed no obvious secondary phase, and the films displayed room temperature ferromagnetism (Fig. 1.6). This MBE study showed that $Ga_{1-x}Gd_xN$ films grown at 700°C with $x > 7.8$ % result in the formation of secondary phases such as GdN as well as reduction of the net magnetization per unit volume as GdN has a T_C of 58 K. Extended X-ray absorption fine structure analyzed data showed that the Gd atoms were primarily incorporated on Ga site. The MBE grown $Ga_{1-x}Gd_xN$ (x = 12.5 %) displayed a saturation magnetization of 320 emu/cm^3 resulting in a magnetic moment of 6.4 μ_B/Gd atom. The saturation magnetization was enhanced by 6 times upon Si doping of $Ga_{1-x}Gd_xN$ (x = 8.9 %) resulting in an increase in saturation magnetization from 137 emu/cm^3 to 1046 emu/cm^3 [66]. Zhou et al. also attribute the magnetization in $Ga_{1-x}Gd_xN$ films to nitrogen vacancies, which can be enhanced by doping with donors.

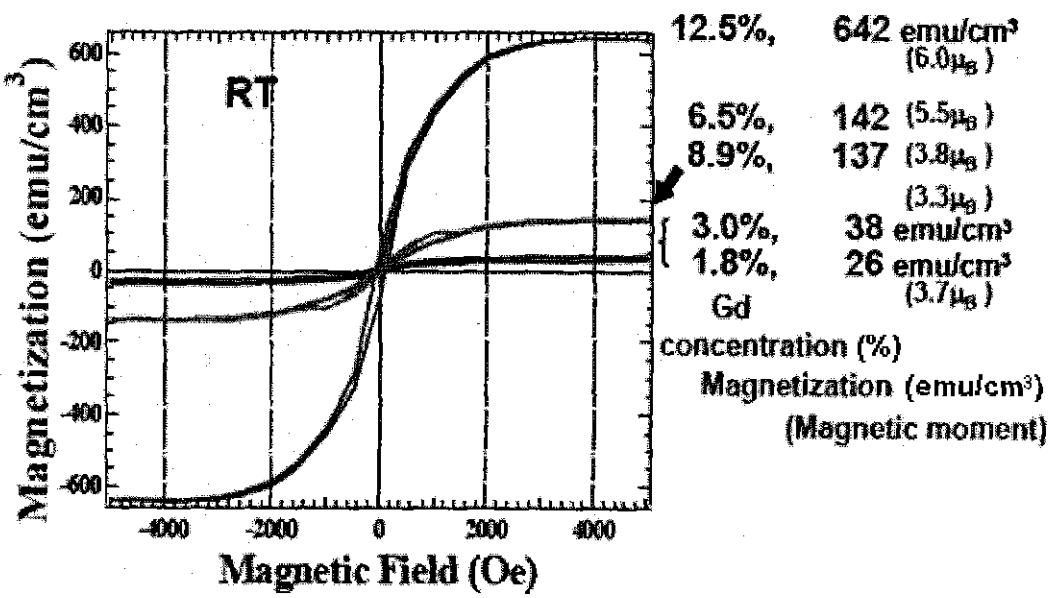

Fig. 1.6 Room temperature *M-H* curves for the $Ga_{1-x}Gd_xN$ layers (x = 1.8-12.5 %) grown at 300°C. The Gd compositions, magnetizations and magnetic moment are listed on the right side [66].

1.2.2 Theoretical models

$Ga_{1-x}Gd_xN$ is promising as it has the potential to be doped with donors (acceptors) with a concentration exceeding that of Gd (concentration of $< 10^{16}$ cm^{-3}) to generate spin-polarized electrons (holes) in the conduction band (valence band), which could be applied to spintronic devices [64, 67]. To date, there is no consistency in the mechanism proposed for the observed magnetism in $Ga_{1-x}Gd_xN$ thin films. The first reports on ferromagnetic $Ga_{0.94}Gd_{0.06}N$ by Teraguchi *et al.* attributed the magnetism to the RKKY-type interaction through the spin-polarized valence band of GaN [68]. Dhar *et al.* attributed the large magnetic moment observed to the long range spin of the GaN matrix incorporated with Gd atoms [69]. On the other hand, MBE reports by Zhou *et al.* predict that electrons introduced by Si doping or defects (nitrogen vacancies) help to stabilize the ferromagnetic phase in $Ga_{1-x}Gd_xN$ films as they offer electrons that couple between the Gd f and host s states [70].

Dalpian and Wei have performed *ab initio* band structure calculations and determined the density of states (DOS) for zinc blende $Ga_{1-x}Gd_xN$ for x = 6.25 % [67]. Their calculations show that the coupling between Gd atoms in zinc blende $Ga_{1-x}Gd_xN$ is antiferromagnetic as the spin-splitting in the ferromagnetic phase does not result in energy gain as compared to the unsplit antiferromagnetic phase. The antiferromagnetic phase is stabilized through superexchange interactions between the Gd 4f and N 2p states. The theoretical calculations show that the addition of electrons can stabilize the ferromagnetic phase as the s-f coupling results in a negative spin exchange splitting [67]. Dalpian and Wei predict that both holes and electrons will result in ferromagnetic interaction in $Ga_{1-x}Gd_xN$ but the electrons are more efficient in stabilizing the ferromagnetic phase and should result in larger magnetic moments.

Recently, first principle calculations based on spin density functional theory have resulted in the electronic structure for wurtzite $Ga_{1-x}Gd_xN$ (x = 12.5 %) shown in Fig. 1.7 [71, 72]. In this model, the 7.4 eV broad valence band is of N 2p character and the conduction band is predominantly formed by the 4s Ga electrons. According to

Hejtmanek *et al.*, the 4f orbitals spin-up band is positioned at -3.5 eV below the valence band maximum and the spin-down states are at 6 eV above the conduction band minimum [71]. The substitution of Ga by Gd is isovalent and thus no electrons or holes are created. Their findings suggest that ferromagnetism in $Ga_{1-x}Gd_xN$ is caused by the RKKY exchange mechanism and is mediated through itinerant carriers that occur due to excitation from an impurity band to the conduction band or due to an impurity band in the degenerate semiconductor [73]. Unlike TM doped GaN, which exhibits metallic or semi-metallic states the $Ga_{1-x}Gd_xN$ system is always a semiconductor with the bandgap gradually decreasing with an increase in Gd concentration [52]. First principle calculations by Zhong *et al.* show that the Fermi level of $Ga_{1-x}Gd_xN$ is always located at the maximum position of the valence band for different Gd concentrations (x ranging from 0.03 to 0.25) [52].

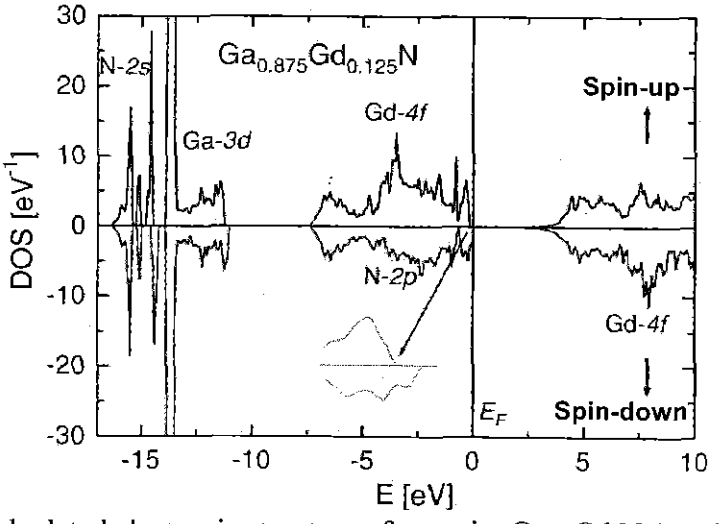

Fig. 1.7 Calculated electronic structure of wurtzite $Ga_{1-x}Gd_xN$ (x = 12.5 %) [71].

Several theoretical analyses have been performed to determine the validity of the long range polarization of the GaN lattice by Gd atoms [52, 67, 73]. These calculations show that the net spin exchange splitting in the valence band or conduction band for RE doped GaN is smaller than that of TM doped, as the f-s, f-p, and f-d couplings in GaN are weaker than that of the d-s, d-d, and d-p hybridization in $Ga_{1-x}TM_xN$. Thus more Gd atoms enhance the magnetic coupling through N atoms, and these N atoms are visibly

polarized in the presence of Gd atoms, but this polarization is too small to result in the large magnetic moment of 4000 μ_B/Gd atom [52, 64].

Unlike other DMS, Gd in GaN has both partially filled 5d and 4f electrons that can contribute to the magnetic moment of Gd, thus it is essential to analyze the effect of both of these orbitals on the ferromagnetism. Spin density functional theory calculations have been performed by Liu *et al.* to determine the magnetism mechanism in $Ga_{1-x}Gd_xN$ [73]. Their findings suggest that the 4f orbitals are too far apart from the valence band maximum (VBM) and conduction band minimum (CBM), and their coupling with free carriers should be weak. Thus, they explored the impact of the Gd 5d electrons. The five-fold degenerate 5d orbitals of Gd are split by the tetrahedral field of the GaN lattice into two e_g and three t_{2g} states. The lowest conduction band of GaN is mainly s-like in character and has very little d character and thus the s-d coupling is expected to be weak as long as the Gd local environment has T_d symmetry. In wurtzite samples, defects and the hexagonal symmetry can result in s-d coupling. On the other hand, relatively flat Gd 5d orbitals with t_{2g} symmetry occur around the p-like VBM of GaN. As the Gd 5d t_{2g} have the same symmetry as the GaN VBM at zone center, the p-d hybridization is very strong as observed in Mn doped GaAs. The energy difference between the ferromagnetic and antiferromagnetic configurations was found to be zero for the structure used in this model; suggesting that $Ga_{1-x}Gd_xN$ should be paramagnetic unless defects exist that stabilize the ferromagnetism. Due to the larger atomic radius of Gd as compared to Ga it is expected that a large density of vacancies exist that could be responsible for the observed ferromagnetism [72, 73].

The two possible scenarios are nitrogen vacancies and gallium vacancies. Nitrogen vacancies (V_N) introduce three conduction electrons to the system and cause the Fermi level to shift well above the VBM. As the local symmetry now allows s-d coupling, the lowest conduction band will contain significant d-character and thus have a significant density of states (DOS) occurring at the Fermi level. The energy difference between ferromagnetic (FM) and antiferromagnetic (AFM) phase, $\Delta E = E_{FM} - E_{AFM}$ for Gd_{Ga} - V_n (Gd_{Ga} = Gd ions replacing Ga) complex is 3.9 meV/Gd atom and implies that

s-d coupling is rather weak. The $\Delta E=E_{FM}-E_{AFM}$ for the wurtzite structure is on the order of -0.7 meV/Gd atom. Liu *et al.* state that the n-type carriers cannot be responsible for the large magnetic moment of 4000 μ_B/Gd atom observed by Dhar *et al.* [64]. In the case of gallium vacancy (V_{Ga}), the missing Ga atom contributes three holes, and the d-band DOS near the Fermi level shows noticeable difference between the spin-up and spin-down states (Fig. 1.8). The calculated energy difference between FM and AFM phase, $\Delta E=E_{FM}-E_{AFM}$ by Liu *et al.*, is -697.1 meV/Gd atom [73]. Their calculations show that a strong FM p-d exchange coupling exists is 180 times stronger than s-d coupling.

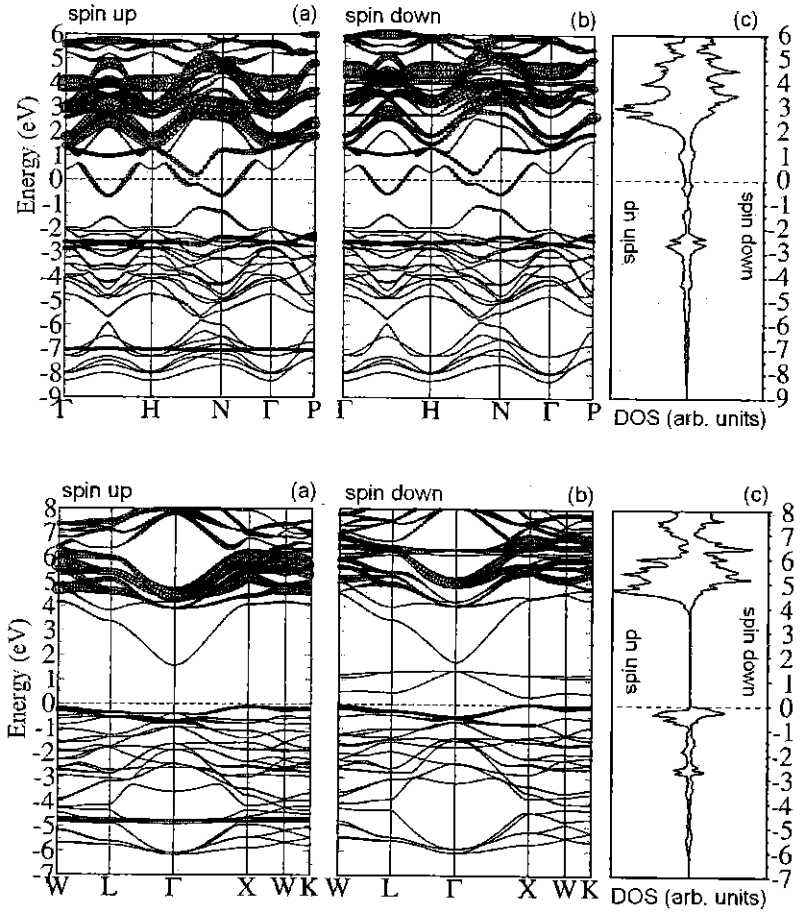

Fig. 1.8 Calculated band structure for (a) spin up, (b) spin down, and (c) d-orbital DOS for $Ga_{1-x}Gd_xN$ in the ferromagnetic (FM) configuration; without Ga vacancy (upper panels) and with Ga vacancy (lower panels) [73].

The p-d exchange is so strong that three unoccupied spin-down valence bands from GaN matrix are pushed above the VBM of the spin-up states resulting in the magnetic moment of the Gd d electron being spread over the p bonding orbital. The calculated ΔE_{FM}-E_{AFM} is -326.1 meV/Gd atom for the super-cell unit for a Ga vacancy. The FM p-d exchange in $Ga_{1-x}Gd_xN$ (for both wurtzite and zinc blende) is over 2 orders of magnitude stronger than the s-d exchange, which implies that holes are more effective than electrons in contributing to the ferromagnetism [73].

Theoretical studies by Gohda *et al.* suggest that the 5d electrons participate in nitrogen bonding and do not contribute to the magnetic moment. Their findings reveal that Gd incorporation causes Ga vacancies and the formation of defect complexes between Ga and Gd atoms are energetically favorable and result in ferromagnetic interactions (Fig. 1.9) [72]. In the absence of V_{Ga}, the magnetic moment comes from the 4f electrons (7 μ_B), and for each V_{Ga} the magnetic moment increases monotonically by 3 μ_B. Overall, this report suggests that the large magnetism observed is due to V_{Ga} that introduce holes above the VBM and implies that holes are responsible for the large magnetization. It must be pointed out that all theoretical models reported to date have been developed to explain the experimental observation of the large magnetic moment in the $Ga_{1-x}Gd_xN$ films grown by Dhar *et al.* [64].

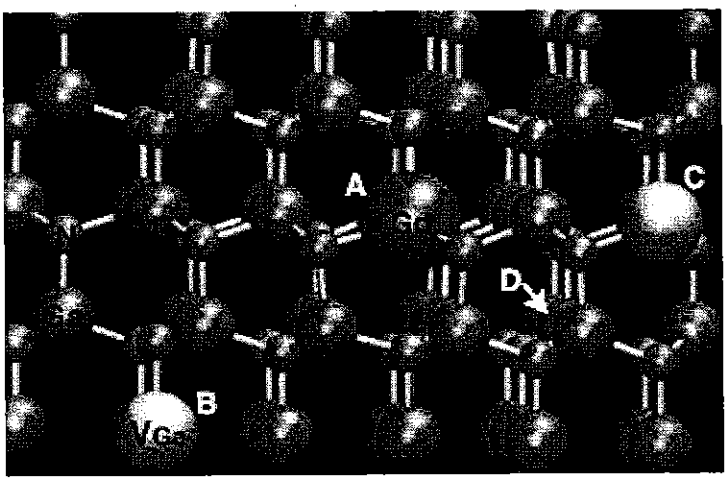

Fig. 1.9 Atomic structure of $Ga_{1-x}Gd_xN$ with the incorporation of Ga vacancy (V_{GA})[72].

1.3 Purpose of this study

The purpose of this study is to examine the feasibility of rare-earth Gd-doped InGaN/GaN magnetic semiconductor heterostructures in search of new functional DMSs for their potential application in long wavelength spin-controlled photonic devices. Semiconductor epilayers and multiple-quantum well structures are grown by plasma-assisted molecular-beam epitaxy (PA-MBE) and explorations on material characterizations are preceded specifically as follows:

(i) Growth and characterization of Gd-doped InGaN, aiming to obtain a room temperature DMS.

(ii) Growth and characterization of Gd-doped InGaN/GaN multiple-quantum well (MQW) to improve the magnetization.

(iii) Growth and characterization of Si co-doping of InGaGdN epilayers and into barrier layers of InGaGdN/GaN MQWs in order to investigate the effect of Si on their characteristics.

This thesis comprises six chapters including this chapter 1.

Chapter 2 describes the experimental methods used in this study. Plasma assisted molecular beam epitaxy was mainly used for the growth of Gd-doped InGaN epilyers and MQW structures. The MBE-grown samples were characterized by X-ray diffraction (XRD), atomic force microscopy (AFM), electron probe micro-analyzer (EPMA), X-ray absorption fine structure (XAFS), photoluminescence (PL), superconducting quantum interference device (SQUID) magnetometer, alternating gradient magnetometer (AGM) and Hall effect measurements. Each of the experimental methods and the basic principles are described.

Chapter 3 describes the successful growth of InGaGdN with Gd concentration of 1~6% by PA-MBE without secondary phases such as GdN, InN as well as the Gd

metallic nanoclusters within the X-ray diffraction detection limit. The optical and magnetic properties of this type of quaternary alloy are further discussed.

Chapter 4 describes the growth and characterization of Gd-doped InGaN/GaN MQW structures. Results indicating the improvement on the magnetic properties achieved by implementing the multiple layer structures of InGaGdN/GaN are discussed.

Chapter 5 describes the effect of Si-doping on the characteristics of InGaGdN epilayers and InGaGdN/GaN MQWs. Enhancement in the magnetic and electrical properties through the incorporation of extra shallow donors by intentionally co-doping the epilayers and the barrier layers of MQW structures is expected.

Chapter 6 describes the overall conclusion of this study.

References

[1] B. G. Streetman, *Solid state electronic devices*, 4th ed. (Prentice Hall, Englewood Cliffs, N.J.,1995).

[2] S. Nakamura, G. Fasol, and S. J. Pearton, *The blue laser diode : the complete story*, 2nd edition. (Springer, Berlin; London, 2000).

[3] S. Datta and B. Das, App. Phys. Lett. **56,** 665 (1989).

[4] G. A. Prinz, Phys. Today **48,** 58 (1995).

[5] S. Gardelis, C. G. Smith, C. H. W. Barnes, E. H. Linfield, and D. A. Ritchie, Phys. Rev. B **60,** 7764 (1999).

[6] P. R. Hammar, B. R. Bennet, M. J. Yang, and M. Johnson, Phys. Rev. Lett. **83,** 203 (1999).

[7] T. Dietl, H. Ohno, F. Matsukura, J. Cibert, and D. Ferrand, Science **287,** 1019 (2000).

[8] C. Liu, F. Yun, and H. Morkoc, J. Mat. Sci.-Mat. in Electron. **16,** 555 (2005).

[9] I. Vurgaftman and J. R. Meyer, J. Appl. Phys. **94** 3675 (2003).

[10] G. A. Prinz, Science **282,** 1660 (1998).

[11] H. Munekata, H.Ohno, S. von Molnar, A. Segmuller, L.L. Chang, and L. Esaki, Phys. Rev. Lett. **63,** 1849 (1989).

[12] H. Ohno, H. Munekata, S. Vonmolnar, and L. L. Chang, J. App. Phys. **69,** 6103 (1991).

[13] H. Ohno, H. Munekata, T. Penney, S. Vonmolnar, and L. L. Chang, Phys. Rev. Lett. **68,** 2664 (1992).

[14] T. Story, R. R. Galazka, R. B. Frankel and P. A. Wolff, Phys. Rev. Lett. **56**, 777 (1986).

[15] H. Akai, Phys. Rev. Lett. **81,** 3002 (1998).

[16] H. Ohno, A. Shen, F. Matsukura, A. Oiwa, A. Endo, S. Katsumoto, and Y. Iye, App. Phys. Lett. **69,** 363 (1996).

[17] H. Ohno, Jpn. J. Appl. Phys. **32,** 459 (1993).

[18] H. Ohno and F. Matsukura, Solid State Commun. **117,** 179 (2001).

[19] H. Ohno, F. Matsukura, A. Shen, Y. Sugawara, N. Akiba, and T. Kuroiwa, Physica E **2,** 904 (1998).

[20] F. Matsukura, H. Ohno, A. Shen, and Y. Sugawara, Phys. Rev. B **57,** R2037 (1998).

[21] Y. Satoh, N. Inoue, Y. Nishikawa, and J. Yoshino, Proc. 3rd Symposium on Physics and Application of Spin-Related Phenomena in Semiconductors, (Sendai, Japan, 1997) p. 23.

[22] T. Dietl, H. Ohno, and F. Matsukura, Phys. Rev. B **63,** 195205 (2001).

[23] H. Ohno, Science **281,** 951 (1998).

[24] J. Szczytko, A. Twardowski, K. Swiatek, M. Palczewska, M. Tanaka, H. Hayashi, and K. Ando, Phys. Rev. B **60,** 8304 (1999).

[25] S. Koshihara, H. Munekata, A. Oiwa, M. Hirasawa, S. Katsumoto, Y. Iye, C. Urano, and H. Takagi, Physica E **2,** 417 (1998).

[26] S. Koshihara, A. Oiwa, M. Hirasawa, S. Katsumoto, Y. Iye, C. Urano, H. Takagi, and H. Munekata, Phys. Rev. Lett. **78,** 4617 (1997).

[27] H. Munekata, T. Abe, S. Koshihara, A. Oiwa, M. Hirasawa, S. Katsumoto, Y. Iye, C. Urano, and H. Takagi, J. App. Phys. **81,** 4862 (1997).

[28] J. Szczytko, A. Twardowski, M. Palczewska, R. Jablonski, J. Furdyna, and H. Munekata, Phys. Rev. B **63,** 085315 (2001).

[29] A. J. Blattner and B. W. Wessels, J. Vac. Sci. Technol. **20,** 1582 (2003).

[30] M. van Schilfgaarde and O. N. Mryasov, Phys. Rev. B **63,** 233205 (2001).

[31] D. Ferrand, A. Wasiela, S. Tatarenko, J. Cibert, G. Richter, P. Grabs, G. Schmidt, L. W. Molenkamp, and T. Dietl, Solid State Commun. **119,** 237 (2001).

[32] T. Dietl, M. Sawicki, L. v. Khoi, J. Jaroszynski, P. Kossacki, J. Cibert, D. Ferrand, S. Tatarenko, and A. Wasiela, Physica Status Solidi B **229,** 665 (2002).

[33] R. Fiederling, M. Keim, G. Reuscher, W. Ossau, G. Schmidt, A. Waag, and L. W. Molenkamp, Nature **402,** 787 (1999).

[34] K. Sato and H. Katayama-Yoshida, Hyperfine Interactions **136,** 737 (2001).

[35] H. Akai, T. Kamatani, and S. Watanabe, Jpn. J. Appl. Phys. **69,** 119 (2000).

[36] T. Kamatani and H. Akai, Physica E **10,** 157 (2001).

[37] H. Ohno, A. Shen, F. Matsukura, A. Oiwa, A. Endo, S. Katsumoto, and Y. Iye, App. Phys. Lett. **69,** 363 (1996).

[38] H. Munekata, H. Ohno, R. R. Ruf, R. J. Gambino, and L. L. Chang, J. Crystal Growth **111,** 1011 (1991).

[39] M. L. Reed, M. K. Ritums, H. H. Stadelmaier, M. J. Reed, C. A. Parker, S. M. Bedair, and N. A. El-Masry, Mat. Lett. **51,** 500 (2001).

[40] M. L. Reed, N. A. El-Masry, H. H. Stadelmaier, M. K. Ritums, M. J. Reed, C. A. Parker, J. C. Roberts, and S. M. Bedair, App. Phys. Lett. **79,** 3473 (2001).

[41] M. E. Overberg, C. R. Abernathy, S. J. Pearton, N. A. Theodoropoulou, K. T. McCarthy, and A. F. Hebard, App. Phys. Lett. **79,** 1312 (2001).

[42] S. Sonoda, S. Shimizu, T. Sasaki, Y. Yamamoto, and H. Hori, J. Cryst. Growth **237-239,** 1358 (2002).

[43] D.A.B. Miller, S. D. Smith, and A. Johnston, Appl. Phys. Lett. **35**, 658 (1979).

[44] M. H. Kryder, IEEE Trans. Magn. **25**, 4358 (1989).

[45] Y. Ohno, D. K. Young, B. Beschoten, F. Matsukura, H. Ohno, and D. D. Awschalom, Nature **402,** 790 (1999).

[46] M. H. Ham, S. Yoon, Y. Park, L. Bian, M. Ramsteiner, and J.-M. Myoung, J. Phys.: Condens. Matter **18,** 7703 (2006).

[47] N. Rangaraju, J. A. Peters, and B.W. Wessels, Phys. Rev. Lett. **105**, 117202 (2010)

[48] A. Punnoose, K. M. Reddy, J. Hays, A. Thurber, and M. H. Engelhard, Appl. Phys. Lett. **89**, 112509 (2006)

[49] T. Aytur, J. Foley, M. Anwar, B. Boser, E. Harris and P.R. Beatty, J. Immunol. Methods **314**, 21 (2006).

[50] M. C. Debnath, V. Zayets and K. Ando, Appl. Phys. Lett. **91**, 043502 (2007).

[51] S. Sugahara and M. Tanaka, J. Appl. Phys. **97**, 10D503 (2005).

[52] G. H. Zhong, J. Lwang, and Z. Zeng, J. Phys-Cond.Matt. **20**, 295221 (2008).

[53] A. J. Steckl, J. C. Heikenfeld, D. S. Lee, M. J. Garter, C. C. Baker, Y. Q. Wang, and R. Jones, IEEE Journal of Selected Topics in Quantum Electronics **8**, 749 (2002).

[54] A. J. Steckl, J. Heikenfeld, D. S. Lee, and M. Garter, Mat. Sci.and Eng. B **81,** 97 (2001).

[55] A. J. Kenyon, Progress in Quant. Electron. **26**, 225 (2002).

[56] R. Birkhahn, R. Hudgins, D. Lee, A. J. Steckl, R. J. Molnar, A. Saleh, and J. M. Zavada, J. Vac. Sci. Technol. B **17**, 1195 (1999).

[57] V. F. Motsnyi, P. Van Dorpe, W. Van Roy, E. Goovaerts, V. I. Safarov, G. Borghs, and J. De Boeck, Phys. Rev. B **68**, 245319 (2003).

[58] Y. K. Zhou, M. Takahashi, S. Emura, S. Hasegawa, and H. Asahi, J. Supercond. Nov. Magn. **23**, 103 (2010).

[59] N. Teraguchi, A. Suzuki, Y. Nanishi, Y. K. Zhou, M. Hashimoto, and H. Asahi, Solid State Commun. **122**, 651 (2002).

[60] D. X. Li, Y. Haga, H. Shida, T. Suzuki, Y. S. Kwon, and G. Kido, J. Phys.-Cond. Matt. **9**, 10777(1997).

[61] P. Heller, Reports on Progress in Physics **30**, 731 (1967).

[62] F. Leuenberger, A. Parge, W. Felsch, K. Fauth, and M. Hessler, Phys. Rev. B **72**, 014427 (2005).

[63] Z. Lipinska, M. Pawlowski, H. Zolnierowicz, A. Wysmolek, M. Palczewska, M. Kaminska, A. Twardowski, M. Bockowski, and I. Grzegory, Acta Phys. Pol. A **110**, 243 (2006).

[64] S. Dhar, L. Perez, O. Brandt, A. Trampert, K. H. Ploog, J. Keller, and B. Beschoten, Phys. Rev. B **72**, 245203 (2005).

[65] J. K. Hite, R. M. Frazier, R. P. Davies, T. Thaler, C. R. Abernathy, S. J. Pearton, J. M. Zavada, E. Brown, and U. Hommerich, J. Electron. Mat. **36,** 391 (2007).

[66] Y. K. Zhou, S. W. Choi, S. Emura, S. Hasegawa, and H. Asahi, App. Phys. Lett. **92**, 062505 (2008).

[67] G. M. Dalpian and S. H. Wei, Phys. Status Solidi B **243**, 2170 (2006).

[68] H. Asahi, Y. K. Zhou, M. Hashimoto, M. S. Kim, X. J. Li, S. Emura, and S. Hasegawa, J. Phys.: Condens. Matter **16,** S5555 (2004).

[69] S. Dhar, O. Brandt, A. Trampert, L. Daweritz, K. J. Friedland, K. H. Ploog, J. Keller, B. Beschoten, and G. Guntherodt, App. Phys. Lett. **82**, 2077 (2003)

[70] Y. K. Zhou, S. W. Choi, S. Kimura, S. Emura, S. Hasegawa, and H. Asahi, J Supercond Nov Magn. **20**, 429 (2007).

[71] J. Hejtmanek, K. Knizek, M. Marysko, Z. Jirak, D. Sedmidubsky, Z. Sofer, V. Perina, H. Hardtdegen, and C. Buchal, J. Appl. Phys. **103**, 07D107 (2008).

[72] Y. Gohda and A. Oshiyama, Phys. Rev. B **78,** 161201 (2008).

[73] L. Liu, P. Y. Yu, Z. Ma, and S. S. Mao, Phys. Rev. Lett. **100**, 127203 (2008).

[74] P. Larson and S. Satpathy, Phys. Rev. B **76,** 8 (2007).